Applied Physics Reviews

RESEARCH ARTICLE | APRIL 26 2024

A generalized model for tribovoltaic nanogenerator

Xin Guo ; Jing You ; Di Wei ; Jiajia Shao ; Zhong Lin Wang

Appl. Phys. Rev. 11, 021415 (2024)
https://doi.org/10.1063/5.0196998

28 April 2024 01:10:04

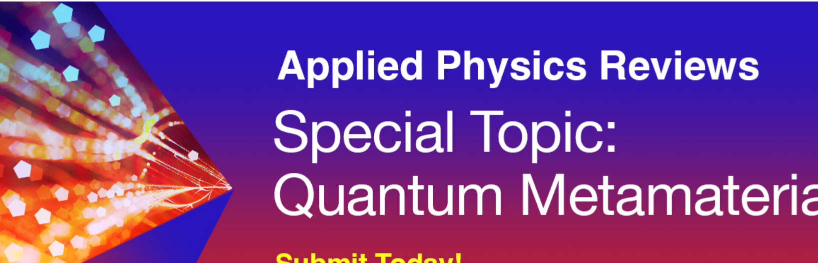

Applied Physics Reviews ARTICLE pubs.aip.org/aip/are

A generalized model for tribovoltaic nanogenerator

Cite as: Appl. Phys. Rev. **11**, 021415 (2024); doi: 10.1063/5.0196998
Submitted: 10 January 2024 · Accepted: 8 April 2024 ·
Published Online: 26 April 2024

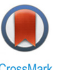

View Online Export Citation CrossMark

Xin Guo,[1,2] Jing You,[1,2] Di Wei,[1,2] Jiajia Shao,[1,2,a)] and Zhong Lin Wang[1,2,3,4,5,a)]

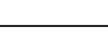

AFFILIATIONS

[1]Beijing Institute of Nanoenergy and Nanosystems, Chinese Academy of Sciences, Beijing 101400, People's Republic of China
[2]School of Nanoscience and Technology, University of Chinese Academy of Sciences, Beijing 100049, People's Republic of China
[3]School of Materials Science and Engineering, Georgia Institute of Technology, Atlanta, Georgia 30332-0245, USA
[4]Guangzhou Institute of Blue Energy, Knowledge City, Huangpu District, Guangzhou 510555, People's Republic of China
[5]Yonsei Frontier Lab, Yonsei University, Seoul 03722, Republic of Korea

[a)]**Authors to whom correspondence should be addressed:** shaojiajia@binn.cas.cn and zlwang@gatech.edu

ABSTRACT

Converting mechanical energy into direct-current electric power based on the tribovoltaic effect is a typical characteristic of tribovoltaic nanogenerators (TVNGs). Although this newly discovered physics effect has been devoted to numerous research studies recently, a generalized theoretical model is still missing, thus unable to comprehensively elaborate the working principles of TVNG. Unlike previous qualitative explanations restricted to the conventional diffusion-drift theory, a new theoretical model is proposed according to classical semiconductor physics. Using the model, the governing equation of a TVNG is derived for the first time, which provides possibilities for revealing the variations of basic physical variables whether within the device or in an external circuit. The direct-current output is suggested to be the coupling of the tribovoltaic effect and contact electrification; in detail, it directly results from the movement and realignment of quasi-Fermi levels for excess carriers that are contiguous to the junction/contacting interface under non-equilibrium conditions. Moreover, an equivalent circuit model is established, equivalent to a constant current source parallel to a p–n junction diode according to the lumped parameter circuit theory. Notably, a new term, mechano-induced electric field $E_{M,}$ is defined and introduced to describe the impact of triboelectric charges at interfaces. Furthermore, using the COMSOL Multiphysics software, a dynamic simulation model for TVNGs is proposed, allowing the simulation and calculation of various TVNGs with different geometric constructions and charge distributions.

Published under an exclusive license by AIP Publishing. https://doi.org/10.1063/5.0196998

28 April 2024 01:10:04

I. INTRODUCTION

Based on the coupling effect of contact electrification (CE) and electrostatic induction, triboelectric nanogenerators (TENGs) can convert mechanical energy into electrical power with an AC signal output in an external circuit.[1–3] The invention of TENGs is a focus question studied at present, which involves in a range of fields such as contact electrification, high entropy energy, self-powered sensors, the Internet of Things (IoT), biological medicine engineering, and so on.[2,4–9] Maxwell's displacement current is regarded as the driving force, owing to the time-varying polarization of dielectrics in TENGs.[1,2] Recent research has shown significant interest in a new kind of energy harvesting device, which is called the tribovoltaic nanogenerator (TVNG) (or direct-current triboelectric nanogenerator).[10–15] A TVNG is constructed of at least the semiconductor materials and electrodes but with a direct current output.[10,14–17] The basic output characteristics and material selection are the important differences between AC-TENGs and TVNGs.[12,17] The physical basis of the latter depends on the triboelectric effect, which results from the electron–hole pairs generated at the p–n junction due to the energy released by the formation of the newly formed chemical bonds at the interface.[18–22] When two semiconductors move toward each other, electron–hole pairs are excited and distributed at the p–n junction/contacting interface.[18,19,23] The generated electron–hole pairs are also referred to as excess carriers. In general, two different forces drive the electrons/holes to drift or diffuse in the space charge region. The first one is the diffuse force, which is created by the density gradients of the carriers. The built-in electric field distributed in the space charge region produces another force on the electrons/holes, which is in the opposite direction to the above diffuse force. Theoretically, all electrons and holes excited are swept out of the depletion region, generating a DC output in the external circuit, along the direction of the built-in electric field but independent of motion direction.[12,18]

Published under an exclusive license by AIP Publishing

The effect of incorporating gallium nitride, telluride, and other materials, as well as heterojunctions, to enhance the output of TVNGs has been investigated, showing results in terms of improving the power generation capabilities.[24–29] Additionally, alternative TVNG structures, such as the p-insulator-n configuration, have been experimentally explored to diversify material options and design possibilities.[30–34] Despite extensive efforts that have been made to improve the basic output performances, either through semiconductor material selection or structure design, there is still an inability to comprehensively clarify the working principles of TVNGs.[18,35,36] This is chiefly because there is still a lack of theoretical models to quantitatively describe relations among physical quantities based on the tribovoltaic effect. In addition, we should pay attention to the triboelectric charges generated at the contacting surfaces of TVNGs, since it is not clear how these charges influence the carrier transport and even working mechanism as well as output characteristics, thus hindering the design and optimization of semiconductor devices for matching application requirements.[10,37] Although very few theoretical physical models are proposed according to drift-diffusion theory, they focus on the junction/interface instead of the whole TVNG device.[38,39] In other words, some local elements have been investigated but not the device physics and device physical model, while the latter is the emphasis.

Here, a theoretical model and analysis for TVNGs are presented, based on the coupling effect of tribovoltaic effect and contact electrification, aiming to capture the in-depth mechanism of the TVNG device. The objective here, first and foremost, is to understand the operation principle, output characteristic, and performance of TVNGs. Deferring the idea above and solar cells theory, we derived the governing equation of TVNGs for the first time. Most importantly, an equivalent circuit model and universal simulation model of a TVNG device are also proposed, offering tremendous possibilities to clarify the underlying mechanisms and quantitative relations among different physical variables. Three typical configurations, namely, ideal p–n junction TVNG, wide-bandgap semiconductor-sandwiched TVNG, and mechano-induced electric field-dominated TVNG, are designed, and numerical experiments are conducted to demonstrate the rationality and validity of these models and theoretical analysis. Detailed investigations are carried out to explore the influences of physical parameters including doping concentration, generation rate of electron–hole pairs, bandgap, as well as geometric parameters on the output performances of TVNGs. The constructed models and theoretical analysis presented here are expected to serve as a potentially powerful tool to better understand the physical mechanism of TVNGs and tribovoltaic effect, which is substantially possible to get its way.

II. GENERAL THEORY

A. The generation of electron–hole pairs and DC-signal

It is important to understand how the electron–hole pairs are generated; here, our focus is to build a theoretical model for TVNGs, revealing how the generated electron–hole pairs flow through the p–n junction/contacting interface and how they flow in the external circuit. A typical AC-TENG device consists of dielectric materials and metal electrodes, using the coupling effect of contact electrification (CE) and electrostatic induction. A traditional lateral-sliding (LS) mode TENG is illustrated in Fig. 1(a). When the reciprocating part (dielectric 1 and the attached top electrode) moves, an alternating current signal is obtained in the external circuit. A typical TVNG consists of at least a semiconductor and two metal electrodes to ensure a dynamic Schottky contact or/and a p–n junction. Unlike the displacement current generation mechanism of AC-TENGs, the physical basis of a TVNG is based on the coupling effect of tribovoltaic effect and contact electrification. For instance, a lateral-sliding TVNG composed of a p-type and an n-type semiconductor is illustrated in Fig. 1(b). As the reciprocating part moves periodically, mechanically induced electron–hole pairs are generated and then redistributed through the p–n junction/contacting interface under driving forces, causing the space charge region formation and destruction simultaneously; as a result, a DC signal is obtained flowing from the p-region (top) electrode through a load resistor in the external circuit to the n-region (bottom) electrode.

B. Energy band diagrams for the dynamic p–n junction

The term tribovoltaic effect is defined to describe the generation of electron–hole pairs at semiconductor interfaces under external mechanical excitation. This special case is similar to the photovoltaic effect, which occurs in solar cells. In solar cell devices, electron and hole pairs are excited by photons, converting solar energy into electricity.[40,41,43] As demonstrated in Fig. 1(d), when photons with energy $h\nu$ exceed the bandgap E_g of the semiconductors, electron–hole pairs are excited within the penetration depth of these photons. The created electron–hole pairs are then separated owing to the built-in electric field. Consequently, the holes move from the n-region to the p-region forming a hole current j_p, while the electrons move from the p-region to the n-region generating an electron current j_n. The working process of TVNGs can be divided into two stages: the contacted stage and the sliding stage. Assume that the semiconductors involved are non-degenerate, satisfying the Boltzmann distribution and neglecting the influence of surface states on the energy band diagram and carrier transport. Figure 1(e) depicts the energy band diagrams and Fermi energy levels for the n-type and p-type semiconductors under thermal equilibrium. When the two semiconductors are brought into contact, the majority carriers of the n-type semiconductor (electrons) and the majority carriers of the p-type semiconductor (holes) diffuse to the opposite side owing to their chemical potential difference. As a result, the negatively charged ions are left in n-type semiconductors and positively charged ions are left in p-type semiconductors, generating a built-in electric field pointing from n-region to p-region. The redistribution of carriers continues until a common flat Fermi level is established through the whole p–n junction [Fig. 1(f)]. At thermal equilibrium, the potential barrier V_{bi} of the p–n junction is determined by[42,43]

$$eV_{bi} = (E_{FN} - E_i) + (E_i - E_{FP}) \approx k_B T \ln \frac{N_D N_A}{n_i^2}, \tag{1}$$

where E_i is the intrinsic Fermi level, E_{FN} and E_{FP} denote the Fermi levels of the n-type semiconductor and p-type semiconductor [Fig. 1(e)], respectively; k_B is the Boltzmann constant, T is the temperature in Kelvin degree, n_i is the intrinsic carrier concentration, which is proportional to $\exp(-E_g/2k_B T)$, and N_D and N_A represent the donor concentration and acceptor concentration, respectively.

For the second step, when the two semiconductors slide relative to each other, the electron–hole pairs are generated due to the triboelectric effect, producing a DC flowing in the external circuit [Fig. 1(g)]. In general, there are two different forces to drive the carriers drift/diffuse in the space charge region. The first kind of force is the

28 April 2024 01:10:04

Published under an exclusive license by AIP Publishing

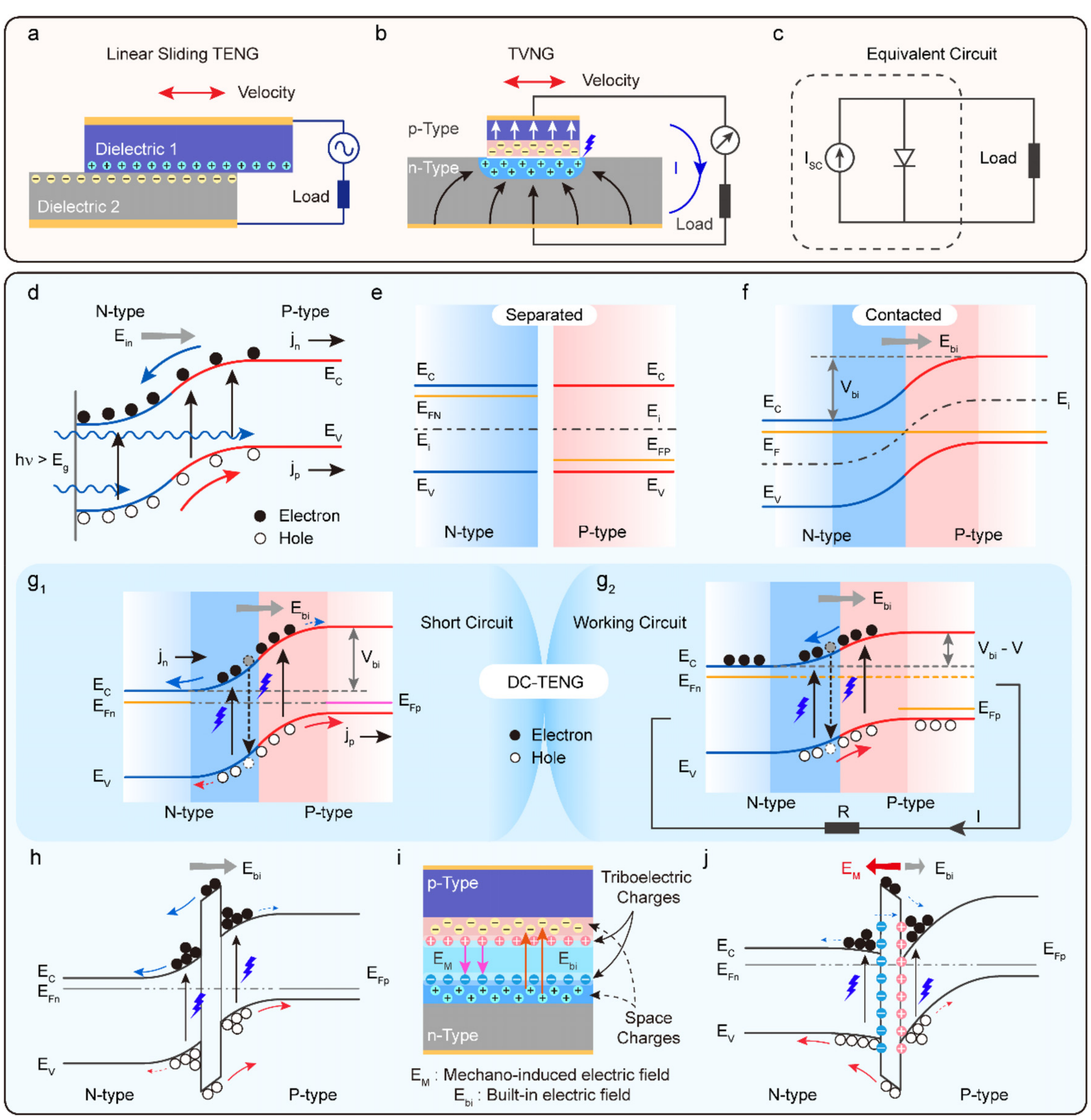

FIG. 1. The TVNG device based on the tribovoltaic effect. (a) Schematic of a linear sliding TENG, which generates an alternating current. (b) Typical structure and (c) equivalent circuit of TVNG based on the tribovoltaic effect. (d) Energy band diagram for a p–n junction solar cell. Energy band diagram for a p–n junction in (e) the separate state and (f) contact state. Energy band diagram for an ideal p–n junction TVNG under (g_1) short-circuit and (g_2) working conditions. (h) Energy band diagrams for a wide-bandgap semiconductor-sandwiched TVNG. (i) The space charges and triboelectric charges near a dynamic p–n junction, and the corresponding built-in electric field as well as mechano-induced electric field. (j) Energy band diagrams for a mechano-induced electric field-dominated TVNG.

diffuse force, which is created by the density gradients of carriers. The built-in electric field distributed in the space charge region produces another force on carriers, which is in the opposite direction to the above diffusion force. After the electron–hole pairs are generated, the holes drift from the n-type to the p-type (red solid arrows), while the electrons drift from the p-type to the n-type (blue solid arrows) under the force produced by the built-in electric field. Another force caused by the carrier concentration gradient acts on the electrons and holes to move in the opposite direction (blue and red dotted arrows). The total effect of the diffuse process and drift process leads to a generation of direct current flowing in the external circuit. Meanwhile, some electrons transit from the conduction band to the valence band, resulting in a reverse process of the electron–hole pair excitation, i.e., recombination (black dotted arrows). There are three main issues that we need to direct our attention to. At short-circuit conditions [Fig. 1(g1)], assume that most of the mechano-induced electron–hole pairs could be swept out of the dynamic p–n junction, and these charges (Q_{SC}) or current (I_{SC}) flow unhindered from the p-type semiconductor electrode to the n-type semiconductor electrode. While at open-circuit conditions, no charges could flow into the external circuit. If an external

28 April 2024 01:10:04

Published under an exclusive license by AIP Publishing

resistor is loaded, only part of the charges can flow from the p-region electrode through the external load to the n-region electrode [Fig. 1(g2)].

C. Equivalent circuit model of TVNGs

Since there is a built-in electric field in the dynamic p–n junction, which points from the n-region to the p-region, the mechano-induced electron–hole pairs are subsequently separated by the electric field. The generated carriers move in the opposite direction: the electrons/holes are injected across the space charge region into the n/p region, which means that the electrons/holes cross the p–n junction where they will flow into the n/p region. As a result, there generates a current in the dynamic p–n junction flowing from the n-region to the p-region (I_M). Consequently, the accumulation of excess holes in the p-region and excess electrons in the n-region results in the growth of electric potential in the p-region and the reduction of electric potential in the n-region. It turns out that the mechano-induced current (I_M) produces a voltage drop (V), which forward biases the p–n junction. The total potential barrier is now reduced to $qV_{bi} - qV$, generating a forward-bias current I_F, which flows in the opposite direction to the I_M. The generation of the I_F can be explained as follows.

Taking Fig. 1(g2) as an example, it shows the energy-band diagram very similar to a case when a forward-bias voltage is applied to the p–n junction. The decrease in the total potential barrier means that the built-in electric field in the space charge region is also decreased. Then, the electrons and holes are no longer held back in the n and p regions, respectively. As a result, the diffusion of holes from the p-region across the p–n junction generates excess minority carriers in the n-region. Again, the diffusion of electrons from the n-region through the p–n junction produces excess minority carriers in the p-region. So, the flow of charges creates a current, which is the forward-bias current I_F. There are three kinds of currents in a TVNG: the mechano-induced current I_M, the forward-bias current I_F, and the conduction current in the external circuit I. Note that both the I_M and I_F flow in the opposite direction. According to the ideal-diode equation, the forward-bias current I_F is written as[42,43]

$$I_F = I_S\left[\exp\left(\frac{eV}{k_B T}\right) - 1\right], \tag{2}$$

where V is the mechano-induced voltage, and I_S represents the reverse-saturation current. If an external resistor is loaded in the external circuit, the conduction current passing through the load is given by

$$I = I_M - I_F = I_M - I_S\left[\exp\left(\frac{eV}{k_B T}\right) - 1\right]. \tag{3}$$

This equation indicates the I–V characteristic of TVNGs. The source I_M results from the excitation of excess carriers by mechanical stimulation. To simply assume the average generation rate (Δg) of non-equilibrium carriers in diffusion lengths ($L_N + L_P$), both the generated holes and electrons, which are distributed in the n-region and p-region with the diffusion length of L_N, L_P respectively, could be across the p–n junction and flows into the other region. Then, the I_M could be written by

$$I_M = q\Delta g S(L_N + L_P), \tag{4}$$

where q is the electron charge, and S is the area of the p–n junction. There are other two cases that deserve serious consideration. First, when there is no external resistor, $V = 0$. The current, in this case, is referred to as the short-circuit current

$$I = I_{SC} = I_M. \tag{5}$$

Another case is when an external resistor goes to infinity, the net current decreases to zero, then one obtains the open-circuit voltage V_{OC}. The mechano-induced current I_M is just balanced by the forward-biased junction current[42,43]

$$I = 0 = I_M - I_S\left[\exp\left(\frac{eV}{k_B T}\right) - 1\right], \tag{6}$$

then the open-circuit voltage V_{OC} is obtained by

$$V_{OC} = \frac{k_B T}{e}\ln\left(1 + \frac{I_M}{I_S}\right) \approx \frac{k_B T}{e}\ln\left(\frac{I_M}{I_S}\right). \tag{7}$$

A plot of the diode currents I as a function of the diode voltage V from Eq. (9) is shown in Fig. 2(g), by which one gets the short-circuit current and open-circuit voltage points on the figure. For a regular p–n junction, the ideal saturation current is given by[42–44]

$$I_S = SqN_C N_V\left(\frac{1}{N_A}\sqrt{\frac{D_n}{\tau_n}} + \frac{1}{N_D}\sqrt{\frac{D_p}{\tau_p}}\right)\exp\left(\frac{-E_g}{k_B T}\right). \tag{8}$$

It is found that the I_S decreases exponentially with E_g, so a large E_g means a large V_{OC} output. Qualitatively, the maximum V_{OC} is the built-in potential of the junction, and the maximum built-in potential is close to the energy gap. This is the internal reason why many experiments have given the conclusion that the V_{OC} is extremely proportional to an energy bandgap E_g.[30,31] In addition, the output power could be given by

$$P = IV = I_M V - I_S V\left[\exp\left(\frac{eV}{k_B T}\right) - 1\right]. \tag{9}$$

The condition of maximum power is obtained when $dP/dV = 0$. From Eq. (9), one has

$$\frac{dP}{dV} = 0 = I_M - I_S\left[\exp\left(\frac{eV_m}{k_B T}\right) - 1\right] - I_S V_m\left(\frac{e}{k_B T}\right)\exp\left(\frac{eV_m}{k_B T}\right) \tag{10}$$

and

$$I_m = I_S\frac{e}{k_B T}V_m\exp\left(\frac{eV_m}{k_B T}\right) \approx I_M\left(1 - \frac{k_B T}{eV_m}\right), \tag{11}$$

$$V_m = \frac{k_B T}{e}\ln\left[\frac{\left(\frac{I_M}{I_S}\right) + 1}{1 + \frac{k_B T}{eV_m}}\right] \approx V_{OC} - \frac{k_B T}{e}\ln\left(1 + \frac{k_B T}{eV_m}\right). \tag{12}$$

The maximum power P_m is then

$$P_m = I_m V_m \approx I_M\left[V_{OC} - \frac{k_B T}{e}\ln\left(1 + \frac{k_B T}{eV_m}\right) - \frac{k_B T}{e}\right]. \tag{13}$$

Assume the input power is P_{in}, then the ideal conversion efficiency η is the ratio of the maximum power output P_m to the incident power P_{in}

28 April 2024 01:10:04

Published under an exclusive license by AIP Publishing

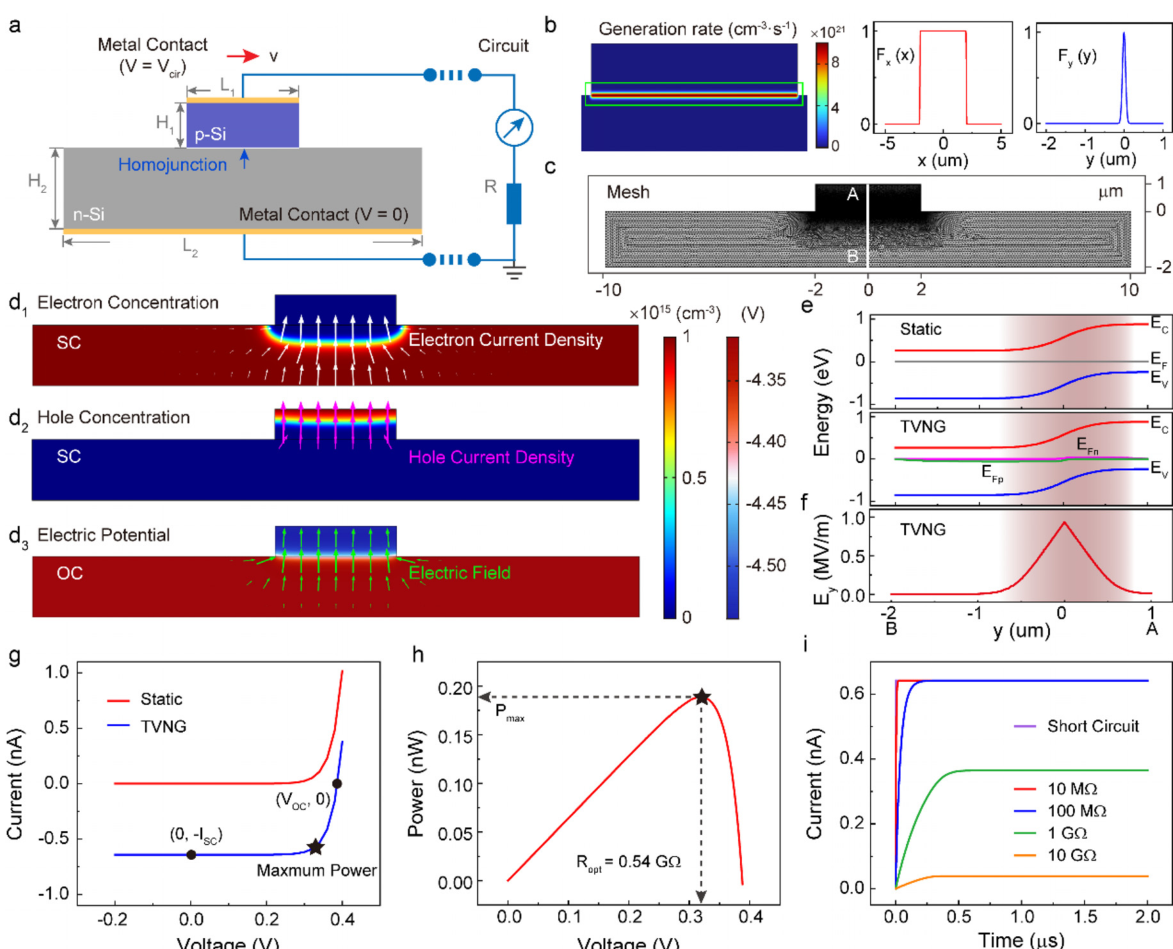

FIG. 2. Finite element simulation and the basic output characteristics of the ideal p–n junction TVNG. (a) Structure diagram and boundary conditions. (b) Mathematical expression of the generation rate of electron–hole pairs. (c) Meshing for finite element simulation. (d_1) Electron concentration and electron current density, (d_2) hole concentration and hole current density under SC condition. (d_3) Electric potential distribution and electric field under OC condition. (e) Comparison of energy bands for static p–n junction and the TVNG at the AB cut line. Quasi-Fermi levels for electrons (E_{Fn}) and holes (E_{Fp}) are introduced to describe excess carriers. (f) Y-component of electric field (E_y) at the AB cut line. (g) *I–V* characteristics of the static p–n junction and the TVNG. (h) *P–V* curve of the TVNG. (i) Output current with time under SC conditions and various loading conditions.

$$\eta = \frac{P_m}{P_{in}} = \frac{I_m V_m}{P_{in}} = \frac{V_m^2 I_S \left(\frac{e}{k_B T}\right) \exp\left(\frac{eV_m}{k_B T}\right)}{P_{in}}. \tag{14}$$

Theoretically, the ideal efficiency can be calculated. It has been found that the mechano-induced current I_M increases with smaller E_g. On the other hand, the voltage increases with E_g by having a small saturation current. Therefore, to maximize the power, there exists an optimal bandgap E_g. According to the lumped parameter circuit theory, a TVNG is equivalent to a constant current source in parallel with a p–n junction in ideal conditions [Fig. 1(c)].

D. Carrier transport in the typical geometric structures

Ideally, the above discoveries could be applied to TVNGs with different geometric structures. When a semiconductor layer with a wide bandgap is inserted between the two semiconductors [Fig. 1(h)], we can predict that the output voltage should be enhanced and even larger than the Fermi level difference between n- and p-type semiconductors owing to the enhancement of interface barrier height. In addition, an increased output voltage means an increased I_F, which decreases the conduction currents I flowing through the external load according to Eqs. (8) and (9). The influence of triboelectric charges distributed on the contacting interface of semiconductors has been carefully noted and investigated. Assume that triboelectric charges are generated and distributed on the contacting interface due to contact electrification [Fig. 1(i)]. The created triboelectric charges make the chemical potential near the p–n junction interface different from that of the bulk regions. Most importantly, the carrier concentration and transport, energy band diagrams, and the built-in electric field can be influenced by the electrostatic charges. The electric field caused by the triboelectric charges on the surface of semiconductors is called the mechano-induced electric field (E_M), which significantly affects the

28 April 2024 01:10:04

Published under an exclusive license by AIP Publishing

basic outputs of TVNGs [Figs. 1(i) and 1(j)]. Refer to Sec. III for the detailed explanations.

III. RESULTS AND DISCUSSION

A. Ideal homogeneous p–n junction TVNG

To make a systematic study of the working mechanism of TVNGs, an ideal homogeneous p–n junction TVNG is designed initially. This TVNG model consists of a stator part including an n-type semiconductor and a (bottom) metal electrode, a sliding part, which is comprised of a p-type semiconductor and a (top) metal electrode, connected to an external electric circuit [Fig. 2(a)]. When there is a relative movement between the n-type and p-type semiconductors, energy releases at the contacting interface leading to a generation of electron–hole pairs. In general, the peak of generation rate occurs at the contacting interface, but it will quickly diminish since the generated electron–hole pairs can inject and diffuse into the bulk of the n- and p-type semiconductors. Here, the generation rate of electron–hole pairs is approximately represented by a mathematical expression $G(x, y, t)$, which is equivalent to a product of a rectangular function $F_x(x)$ with a constant value within the contact region and zero outside the region and a Gaussian function $F_y(y)$ centered at the interface [Fig. 2(b)] as follows:

$$G(x, y, t) = AF_x(x - vt)F_y(y), \quad (15)$$

where A is a coefficient with the unit of $1/(cm^3 \cdot s)$ and v represents the sliding velocity of the sliding part. The corresponding meshes created are illustrated in Fig. 2(c) (see Sec. V and supplementary material for all modeling details). Under SC conditions, the excess holes drift from the n-region through the dynamic p–n junction to the p-region, while the excess electrons drift from the p-region through the dynamic p–n junction to the n-region under the built-in electric field, thus generating a conduction current passing from the n-region to p-region [Figs. 2(d1) and 2(d2)]. The current in the n-region is mainly carried by electrons, and that in the p-region is mainly by holes within the TVNG. Inversely, in the external circuit, the current flows from the top electrode (connected with the p-type semiconductor) to the bottom electrode (connected with the n-type semiconductor). Under OC conditions, there are no chargers transferred between the two electrodes, which makes the electric potentials distributed in the n-type and p-type semiconductors different [Fig. 2(d3)]. It should be noted that the potential inside the DC-TENG is negative since the vacuum energy level is taken as zero in the model. In addition, we know that the thermal-equilibrium electron and hole concentrations are functions of the Fermi energy level. Due to the generated electron–hole pairs and non-equilibrium carriers injected during the relative movement, the quasi-Fermi levels for electrons (E_{Fn}) and holes (E_{Fp}) are introduced to replace the Fermi energy level obtained in equilibrium [Fig. 2(e)]. An electric field is built up caused by the positive ions in the n-side and the negative ions in the p-side, and its direction is in the negative y direction of this geometry [Fig. 2(f)]. The maximum electric field (about 0.93 MV/m) occurs at the contacting interface ($y = 0\,\mu$m) since the concentrations of carriers in the depletion region are much smaller than those distributed outside of the space charge region.

Plots of Eqs. (2) and (3) are demonstrated in Fig. 2(g), which illustrate the I–V characteristic of TVNGs at static and dynamic states, respectively. It is observed that the p–n junction exhibits a rectification characteristic, while at dynamic state, the I–V curve moves downward along the current-axis with a value of I_{SC}. Note that the V_{OC} and I_{SC} are two key parameters of the TVNG, which can be calculated from the current-axis intercept and voltage-axis intercept, respectively. According to Eq. (9), the P–V curve is demonstrated in Fig. 2(h), where the peak of the power is denoted as P_{max} representing the maximum power of the TVNG, and the corresponding loading resistance is regarded as an optimum resistance R_{opt}. When the generation factor A is set as $1 \times 10^{22}\,cm^{-3} \cdot s^{-1}$, the I_{SC} and V_{OC} are 0.642 nA and 0.39 V, respectively, with a maximum power of 0.189 nW under an optimum resistor of 0.54 GΩ of the ideal homogeneous p–n junction TVNG. Moreover, the direct current–time relationships under different external loads are given in Fig. 2(i). Different relaxation times, which are strongly affected by the external circuit conditions, are required for the output currents to reach the steady state [Figs. 2(i) and S2]. Under short-circuit conditions, the relaxation time is very small and is quite negligible owing to without any obstruction for the charges transferring from one electrode to another, while under loading or open-circuit conditions, carriers cannot flow freely, requiring more time for the circuit to reach a steady state.

Furthermore, both the generation rate and doping concentration are researched in detail when we investigate the basic output performances of TVNGs (Fig. 3). Since the net current flows across the dynamic p–n junction, the quasi-Fermi energy levels for the electrons and holes must change. In the regions where the injected non-equilibrium minority carriers are distributed, the quasi-Fermi energy levels of electrons and holes [E_{Fn} and E_{Fp} in Fig. 3(a)] are presented. As the generation rate increases, more minority carriers move from the p–n junction into the neutral semiconductor region, which is far from the space charge region. It should be noticed that the relative change of the majority carrier concentrations is substantially smaller than the corresponding relative change of the minority carrier concentrations. The generation of electron–hole pairs exhibits a limited effect on the majority carrier concentrations but substantially affects the minority carriers. Therefore, the minority carrier concentrations (holes) in the n-region notably increase, making the E_{Fp} closer to the valence band; similarly, the minority carrier concentrations (electrons) in the p-region increase, leading to the E_{Fn} moving to the conduction band [Fig. 3(a)]. The excess minority carrier concentrations become to be zero at distances far from the space charge region. At the edge of the p-region ($y = 1\,\mu$m) and n-region ($y = -2\,\mu$m), both the corresponding E_{Fn} and E_{Fp} are close to 0. According to Eqs. (4) and (7), the I_M and V_{OC} are all proportional to the generation rate. Therefore, the I_M and V_{OC} become bigger as the generation rate increases [Fig. 3(b)], and the peak of the output power (P_{peak}) is also directly proportional to the generation rate.

Figures 3(c) and 3(d) depict the electric potential distribution within the TVNG and I_{SC} and V_{OC} at different doping concentrations. Increasing the doping concentration from $10^{14}\,cm^{-3}$ to $10^{18}\,cm^{-3}$, the electric potential increases from 0.52V to 0.97V accordingly but largely drops in the junction region. According to Eq. (1), it is understood that increasing the doping concentration increases the built-in potential. We further note that the junction width decreases at a higher doping concentration. In general, the total width of the depletion region extending into the p-region and n-region is a reciprocal function of the doping concentration because the depletion region can extend further into the lower-doped region. From Fig. 3(d), we notice that the V_{OC} increases with the increase of the doping concentration, but it has little

28 April 2024 01:10:04

Published under an exclusive license by AIP Publishing

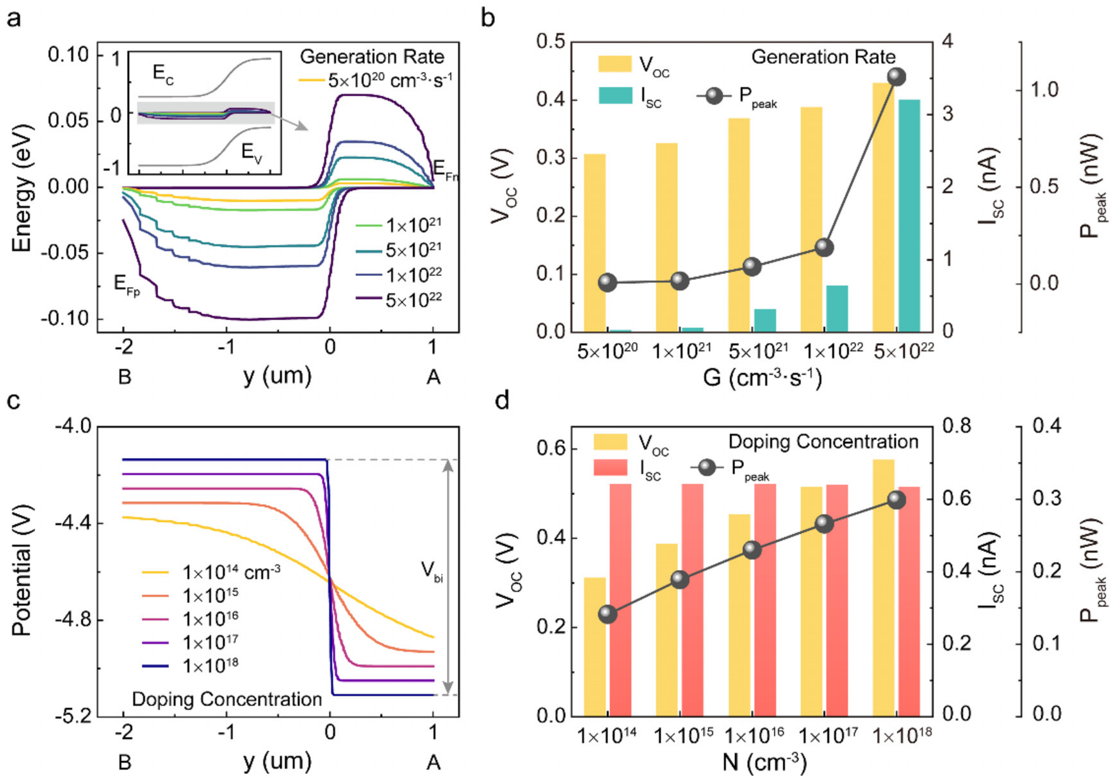

FIG. 3. Effect of the electron–hole pair generation rate and doping concentration. (a) Quasi-Fermi level for electrons and holes (E_{Fn} and E_{Fp}) at the AB cut line with varies electron–hole pair generation rates under SC conditions and (b) the effect of electron–hole pair generation rate on I_{SC}, V_{OC}, and P_{peak}. In these cases, the doping concentration is set as $1 \times 10^{15}\,\text{cm}^{-3}$. (c) Electric potential distribution at the AB cut line with various doping concentrations at the static state, and (d) effect of doping concentration on I_{SC}, V_{OC}, and P_{peak}. In (c) and (d), the generation rate is 1×10^{22} 1/(cm^3·s).

28 April 2024 01:10:04

effect on I_{SC}. Although a larger doping concentration results in a bigger majority carrier concentration, the excess carrier concentration remains limited by the generation rate of electron–hole pairs, which can be found in Eq. (4). However, a larger doping concentration generates a smaller inverse saturation current I_S, and the V_{OC} is inversely and exponentially proportional to the I_S based on Eq. (7). Therefore, a smaller I_S gives rise to a larger V_{OC} output. The corresponding I–V and P–V curves are shown in Figs. S3. A detailed comparison of the theoretical calculations and experimental results are shown in supplementary material Note 5.

B. Wide-bandgap semiconductor-sandwiched TVNG

It has been found that a larger bandgap is beneficial to get a higher V_{OC} of TVNGs.[12,39,45] Now, a wide-bandgap semiconductor is inserted between the n-type and p-type semiconductors to discuss this phenomenon. In general, wide-bandgap semiconductor materials have bandgaps in the range above 2 eV, showing electronic properties that fall in between those of conventional semiconductors and insulators. The schematic diagram of a TVNG based on a wide-bandgap semiconductor sandwiched at the interface is shown in Fig. 4(a). The parameters are listed in Table S2. Note that the inserted wide-bandgap semiconductor is set as a pure semiconductor without any dopant species present. In the static state, this wide-bandgap semiconductor-sandwiched TVNG exhibits rectification characteristics, which are similar to that of an ideal p–n junction [Fig. S5(a)]. When the sliding part moves, the electrons (holes) from the p(n)-region cannot flow freely to the n(p)-region. This is attributed to the fact that the wide-bandgap semiconductor builds up a higher potential barrier in the junction region, which impedes the carriers from diffusing and drifting into each semiconductor material. Only part of the carriers in a higher energy state can cross the potential barrier [Fig. 4(b)]. Figures 4(c) and 4(d) illustrate the carrier distributions and energy band diagrams along the cut line AB. There are two discontinuity energy bands distributed at the conduction band and valence band, respectively, forming heterojunction junctions at the contacting interface between the interfaces of the n-type (and p-type) silicon and the un-doped wide-bandgap semiconductor layer. As demonstrated in Fig. 4(a), the first junction forming at the interface of n-type silicon and wide-bandgap semiconductor is denoted as the left abrupt junction, while the other junction is denoted as the right abrupt junction.

For the Fermi levels in these materials to become aligned, electrons and holes from the narrow-bandgap region must cross the two abrupt junctions. For instance, the electrons from the narrow-bandgap n-region flow into the wide-bandgap silicon. A positive space charge region exists in the narrow-bandgap n-region and an accumulation layer of electrons exists at the interface of the wide-bandgap silicon, creating a built-in electric field pointing from the n-region to the wide-

Published under an exclusive license by AIP Publishing

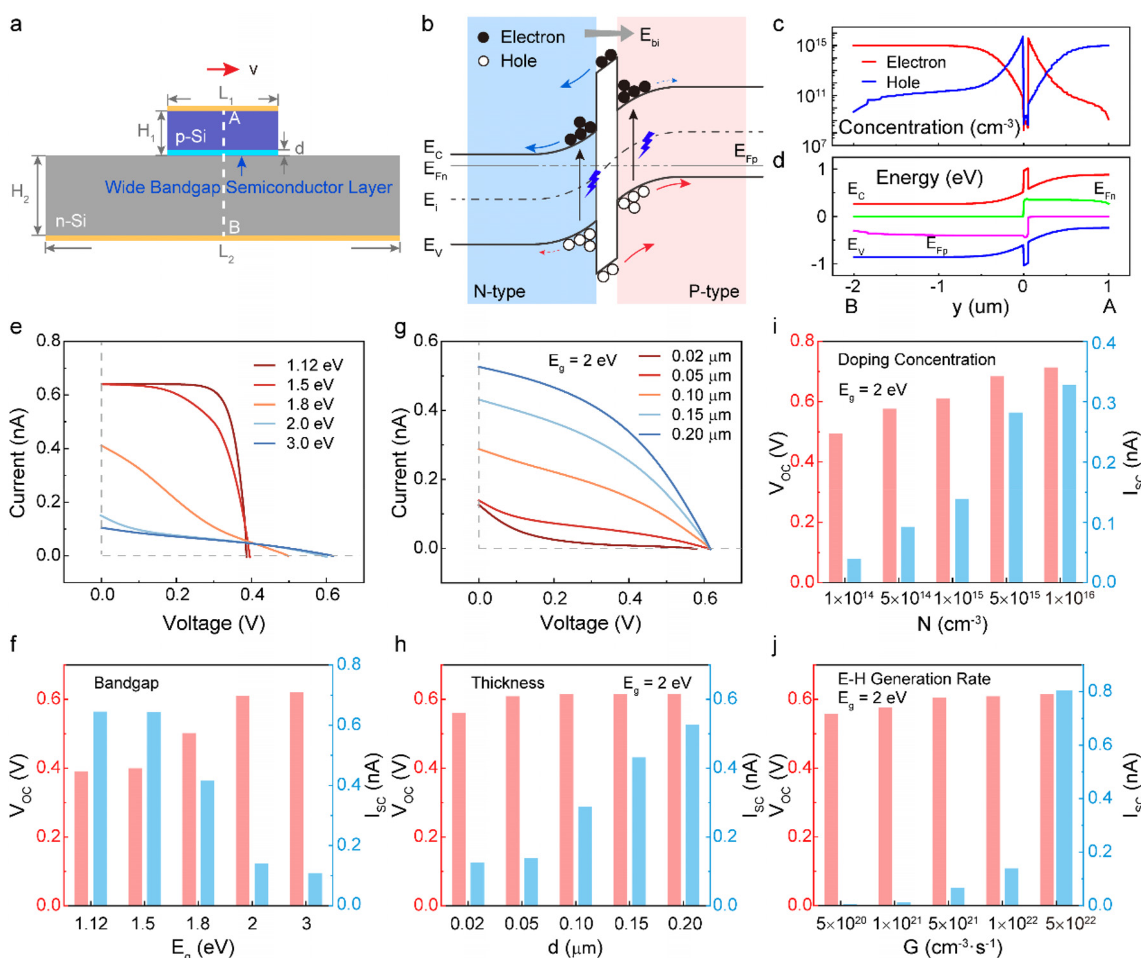

FIG. 4. TVNG based on the wide-bandgap semiconductor-sandwiched structure. (a) Structure diagram. (b) Working mechanism. (c) Carrier concentrations and (d) energy bands at the AB cut line. (e) *I–V* characteristics when the bandgap of the middle layer varies from 1.12 to 3 eV and (f) the corresponding I_{SC} and V_{OC}. (g) *I–V* characteristics when the thickness of the middle layer varies from 0.02 to 0.2 μm and (h) the corresponding I_{SC} and V_{OC}. Effect of (i) doping concentration and (j) electron–hole pairs generation rate on I_{SC} and V_{OC}.

bandgap semiconductor. However, in the wide-bandgap semiconductor, the carrier concentration is extremely smaller since it is un-doped without any dopant species present. As demonstrated in Fig. S5(c), the carrier concentrations are no longer continuous when they meet the wide-bandgap region. However, due to the generated electron–hole pairs, the carrier concentrations distributed in this region are strongly enhanced; the same phenomenon can also be found in the right abrupt junction [Fig. 4(c)]. Note that the generated hoes drift from the wide-bandgap silicon to the n-type silicon owing to the built-in electric field. Therefore, the excess holes decrease gradually by recombination with the majority carrier electrons in the n-region, until they are decreased to a small value when it is far away from the junction. Similarly process for the excess electrons. The carrier concentration leads to a special energy band diagram demonstrated in Fig. 4(d), which unquestionably influences the *I–V* characteristic of the wide-bandgap semiconductor-sandwiched in TVNG.

The changes of current and voltage calculated at different bandgaps are depicted in Figs. 4(e) and 4(f). Increasing the bandgap, the output current decreases but the voltage increases. It is because the carrier transport is suppressed by the inserted wide-bandgap layer, only part of the carriers with high energies could flow across the two abrupt junctions. As a result, a small net charge current flows in the external circuit. In addition, according to Eqs. (7) and (8), V_{OC} is approximately proportional to the bandgap. The thickness of the wide-bandgap layer is another factor that influences the basic outputs of TVNGs. Both the I_{SC} and V_{OC} increase with the thickness of the wide-bandgap semiconductor within a certain range [Figs. 4(g) and 4(h)]. Fig. S7 illustrates the carrier concentrations inside TVNGs with the thickness of the wide-bandgap layer of 0.05 and 0.2 μm, respectively. With the increase in the thickness of the wide-bandgap layer, both the electron and hole concentrations inside have decreased especially in the junction regions. This means that, on the one hand, more generated excess carriers are swept out of the junction regions and injected into the diffusion regions under the built-in electric field for the TVNG with a thicker wide-bandgap layer. On the other hand, the recombination of electrons and holes reduces as increasing the thickness of the wide-

28 April 2024 01:10:04

Published under an exclusive license by AIP Publishing

bandgap layer, due to that the recombination is proportional to the carrier concentrations. Consequently, increasing the thickness of the wide-bandgap layer could inevitably increase the diffusion length of carriers. The current I_M, which is directly proportional to the diffusion length of the non-equilibrium carriers, will become larger. Thus, larger I_{SC} and V_{OC} are obtained. Studies have returned similar results as the p–n junction TVNG when increasing the generation rate and doping concentration [Figs. 4(i) and 4(j)]. As discussed above, the intrinsic reason for these phenomena could be that the sum of the electron and hole currents is significantly enhanced, thus giving rise to a larger output performance of the TVNG.

C. Mechano-induced electric field-dominated TVNG

In general, when two materials are in contact with each other, triboelectric charges are created, generating an electric field perpendicular through the contacting interface. If the case occurs between the p–n junction, there is no doubt that the generated mechano-induced electric field (E_M) can affect the basic outperformances of TVNGs. Such a TVNG is referred to as a mechano-induced electric field-dominated TVNG. If the magnitude of E_M is close to or even larger than that of the built-in electric field (E_{bi}), one cannot neglect the change of the carrier transport process in the dynamic p–n junction and the bulk regions of the n and p semiconductors. The following two situations are discussed in more detail. First, if the generated E_M displays the same direction as the E_{bi}, the total electric field is enhanced, which makes the carriers have a bigger moving velocity, resulting in a larger DC output. However, if the two electric fields go in the opposite direction, the total electric field will be decreased, which then reduces the output voltage and current. It is more likely that if the E_M is extremely larger than the E_{bi}, the carriers will move in the opposite direction, leading to the direct current in the external circuit flowing in the opposite direction.

As demonstrated in Fig. 5(a), triboelectric charges are generated at the contacting interface. The charges distributed on the lower surface of the p-region and the upper surface of the n-region are represented by σ_1 and σ_2, respectively, satisfying the equation of $L_1\sigma_1 + L_2\sigma_2 = 0$ according to electrostatic theory. The I–V characteristic

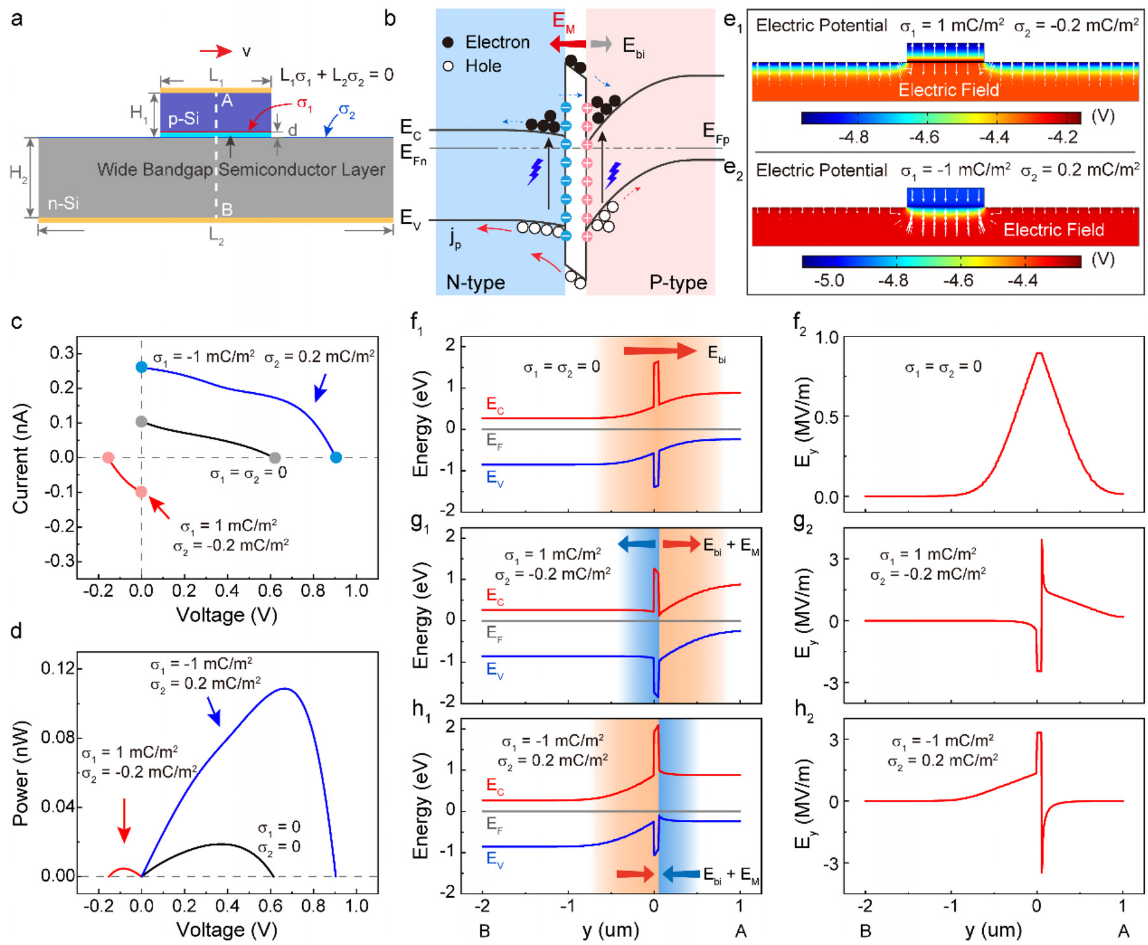

FIG. 5. Mechano-induced electric field-dominated TVNG. (a) Structure diagram and (b) working mechanism. (c) I–V characteristics and (d) P–V curves under three interfacial charge density conditions. (e) Electric potential distribution and electric field under two interfacial charge density conditions. Energy bands and distribution of E_y at the AB cut line when (f) $\sigma_1 = \sigma_2 = 0$, (g) $\sigma_1 = 1$ mC/m^2, $\sigma_2 = -0.2$ mC/m^2, and (h) $\sigma_1 = -1$ mC/m^2, $\sigma_2 = 0.2$ mC/m^2, respectively.

28 April 2024 01:10:04

Published under an exclusive license by AIP Publishing

and corresponding P–V curves under three different charge densities are explored in Figs. 5(c) and 5(d). When $\sigma_1 = \sigma_2 = 0$, the energy band diagram and E_{bi} pointing from the n-side to the p-side are illustrated in Figs. 5(f1) and 5(f2). It is observed that the electron (hole) concentration decreases gradually (increases) from the n-side to the p-side [Fig. S9(a)]. Within the wide-bandgap semiconductor, the carrier concentrations of the electron and hole are abruptly reduced, even close to zero. This case is the same as the case analyzed in detail in Sec. III B. In this case, the I_{SC} is 0.1 nA, and V_{OC} is 0.62 V, with a maximum power of 0.019 nW.

If the lower surface of the p-region and the upper surface of the n-region are charged positively and negatively, respectively. For instance, if one sets $\sigma_1 = 1$ and $\sigma_2 = -0.2$ mC/m^2, it generates a reverse current flowing from n- to the p-region through the external circuit. As illustrated in Fig. 5c, the I_{SC} is -0.1 nA, and V_{OC} is about -0.15 V. The corresponding output power is reduced compared with the case when there are no created triboelectric charges [Fig. 5(d)]. If $\sigma_1 = -1$ and $\sigma_2 = 0.2$ mC/m^2, the basic outputs of the TVNG are significantly increased [Fig. 5(d)]. The electric potential and electric field distribution for the two cases are shown in Figs. 5(e1) and 5(e2). When $\sigma_1 = 1$ and $\sigma_2 = -0.2$ mC/m^2, E_M is generated, pointing from the p-region to the n-region. Then, the electrons are attracted and moved toward the wide-bandgap region, making the electrons accumulate, and the holes are excluded and moved away from the wide-bandgap semiconductor [Fig. S9(b)]. Thus, the potential of the p-region adjacent to the contacting interface is raised and the potential of the n-region is reduced. Consequently, the relevant energy bands bend and the electric field distributed in the n-region within the wide-bandgap layer is negative. So, the excess holes move toward the bottom electrode and excess electrons move toward the p-side, leading to a reverse current flowing in the external circuit. When $\sigma_1 = -1$ and $\sigma_2 = 0.2$ mC/m^2, E_M is generated pointing from the n-region to the p-region. Thus, the holes are attracted and accumulate, but the electrons are depleted [Fig. S9(c)]. Then, a larger positive electric field is generated near the contacting interfaces [Figs. 5(h1) and 5(h2)]. If we consider the difference between the two cases, it can be understood quite easily why there appears an enhancement effect when $\sigma_1 = -1$ and $\sigma_2 = 0.2$ mC/m^2. Against this background, it is very fitting to note that, when the E_M displays the same direction as the E_{bi}, it is beneficial for the excess carriers to transport. Overall, the numerical results indicate that the outputs of the TVNG can be greatly enhanced by the triboelectric charges under special conditions. It can be generally concluded that modifying the charge generation and distribution at the contacting interface can modulate the basic outputs of TVNGs.

Moreover, the influence of the charge density and doping concentration on I_{SC} and V_{OC} are also investigated. Considering the first case, that is, the lower surface of the p-region and the upper surface of the n-region are positively and negatively charged, respectively. A very small charge density ($\sigma_1 = 0.1$ mC/m^2) can make a significant reduction of V_{OC} and I_{SC} [Fig. 6(a)]. This is attributed to the fact that the E_M generated by the triboelectric charges displays an opposite direction compared with E_{bi}, then decreasing the total internal electric field, hindering the movement of carriers. Increasing the charge density σ_1 to 0.5 mC/m^2, there displays a reversed output current and voltage, indicating that the total internal electric field has a reverse direction. As σ_1 continues to increase, the created E_M is larger than that of the original E_{bi}, leading to an enhancement of the reverse basic outputs. If the charge distribution is contrary to the former, both the I_{SC} and V_{OC} increase as the charge density of σ_1 increases [Fig. 6(b)]. The total internal electric field is enhanced in this case. The influence of doping concentration on the basic outputs of TVNGs is demonstrated in Figs. 6(c) and 6(d). Increasing the doping concentration, both the I_{SC} and V_{OC} are decreased and then increased inversely when the charge density of σ_1 is positive. That switch happens under the doping concentration close to 5×10^{15} cm^{-3}[Fig. 6(c)], which is because the E_M is stronger than the E_{bi} at this moment. On the contrary, under the condition of $\sigma_1 = -1$ and $\sigma_2 = 0.2$ mC/m^2, increasing the doping concentration results in larger I_{SC} and V_{OC}.

IV. CONCLUSIONS

In summary, a generalized theoretical model is proposed to elucidate the in-depth mechanism of the TVNG. The built model is universal and can be utilized to comprehensively describe the charge, current, voltage, and power output behaviors in the external circuit, clarifying the dynamic p–n junction, electron–hole separation process, built-in electric field, Fermi levels (and the quasi-Fermi levels), electric field, and electric potential distributions in the "internal circuit." Intentionally referencing the solar cells theory, the governing equation of TVNGs is proposed for the first time, which reaches beyond the conventional diffusion-drift theory-based explanations. A universal simulation model integrative framework is proposed, according to the key theory and technologies of simulation. Using the simulation methods, the basic output performances and influences such as material properties and structural parameters for three typically designed TVNGs are analyzed. The basic conclusions are as follows:

(1) The physical fundament of TVNGs is based on the coupling effect of tribovoltaic effect and contact electrification. Because of the tribovoltaic effect, the electron–hole pairs are generated at the sliding/contacting interface under mechanical excitation, while the electron–hole pair separation process is mainly dominated by the time-varying electric field that is primarily distributed within the dynamic p–n junction. Since the built-in electric field points from the positive to the negative charges, the movement of mechano-induced carriers (electron-hole pairs) generates a DC-current, with the holes flowing to the p-side and electrons flowing to the n-side, respectively. So, the direction of the current within TVNGs is consistent with that of the electric field, which dominates the separation of carriers. Outside the TVNG device, the produced current flows from the p-region through the load resistor to the n-region, regardless of the moving direction.

(2) Different from the traditional Fermi energy level obtained under thermal-equilibrium conditions, the quasi-Fermi levels are applied for non-equilibrium states caused by the mechano-induced (excess) carriers within the TVNG device. As the electron/hole concentration increases or decreases in the depletion region and diffusion region, the quasi-Fermi level for electrons/holes will move slightly closer to/away from the conduction/valence band. The degree of quasi-Fermi level splitting is a measure of the total carrier concentrations under mechanical excitation and illustrates the fact that the electrons flowing through the external circuit have to balance the deviation to maintain thermal equilibrium. This is why there are different changes in the carrier concentration, electric field/potential distribution,

28 April 2024 01:10:04

Published under an exclusive license by AIP Publishing

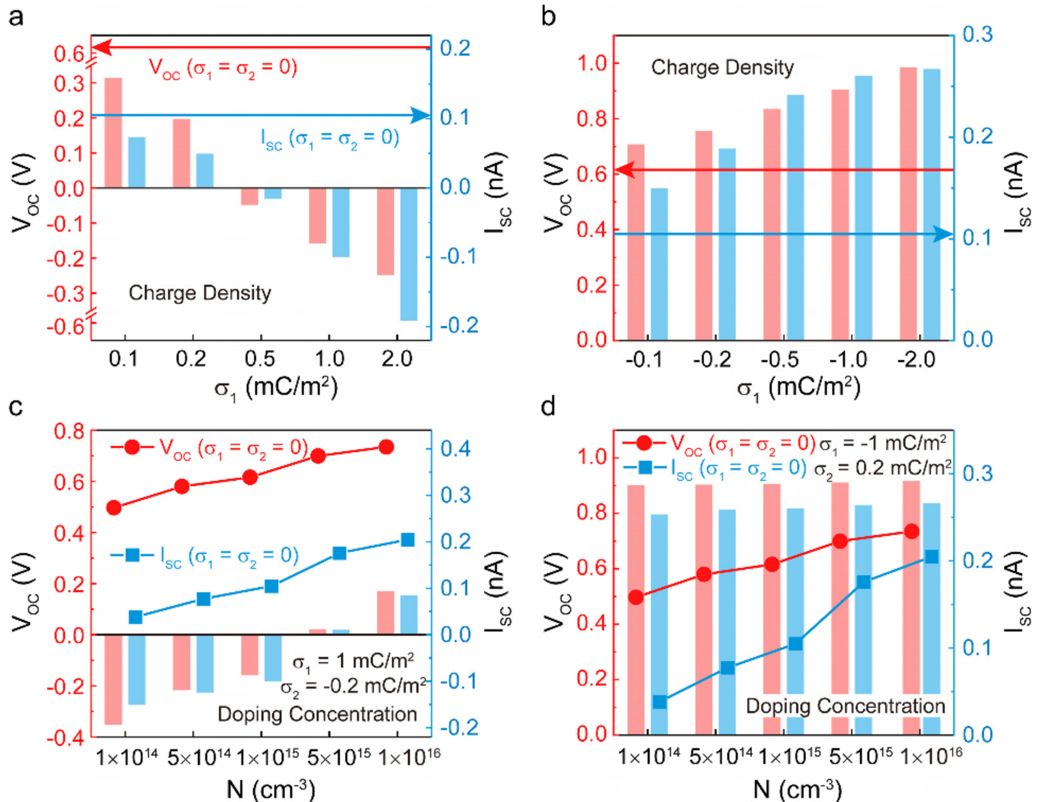

FIG. 6. Effect of charge density and doping concentration on I_{SC} and V_{OC} of the mechano-induced electric field-dominated TVNG. I_{SC} and V_{OC} when σ_1 varies (a) from 0.1 to 2.0 mC/m^2 and (b) from -0.1 to -2.0 mC/m^2. I_{SC} and V_{OC} of the TVNG with various doping concentrations when (c) $\sigma_1 = 1$, $\sigma_2 = -0.2$ mC/m^2, and (d) $\sigma_1 = -1$, $\sigma_2 = 0.2$ mC/m^2.

28 April 2024 01:10:04

and energy band diagrams compared with a traditional p–n junction.

(3) According to the lumped parameter circuit theory, a TVNG is equivalent to a constant current source in parallel with a p–n junction diode theoretically.There are three-type currents in a TVNG: the mechano-induced current I_M flowing from the n-region to the p-region, the forward-bias current I_F flowing from the p-region to the n-region caused by the total potential difference between the two electrodes, and the conduction current in the external circuit I. The I_M and I_F flow in opposite directions. Furthermore, the short-circuit current and open-circuit voltage are essentially determined by the carrier concentrations, the strength, and distribution of the inner electric field, as well as the height of the potential barrier. Increasing the generation rate of electron–hole pairs and doping concentration can significantly enhance the basic outputs. In addition, inserting a wide-bandgap semiconductor between p-type and n-type semiconductors generates a higher barrier adjacent to the junction/interface, which can effectively expand the bandgap, increasing the open-circuit voltage but decreasing the output current.

(4) Contact electrification is a universal phenomenon that occurs almost at any interface. To describe the influence of triboelectric charges created at the contacting interface of semiconductors, a term, that is, mechano-induced electric field $E_{M,}$ is defined. The direction of E_M can be equal or opposite to that of the built-in electric field distributed in the space charge region, depending on the characteristics of semiconductor materials. Therefore, the basic outputs of the TVNG will be enhanced or decreased, which largely depends on the carrier transportation under the coupling effect of E_M and E_{in}.

(5) A dynamic simulation model for the TVNGs is also constructed, using the COMSOL multi-physics software, which includes at least three different modules: electric circuit (cir), semiconductor (semi), and moving mesh (ale). By this universal model, one can simulate and calculate any kind of TVNGs with different geometric constructions and charge distributions. What is worth highlighting is that the simulation model couples the tribovoltaic effect and contact electrification comprehensively, which could become a powerful tool for investigating the relevant sciences and technologies.

V. METHODS

The finite element simulations for the TVNGs with three different configurations [Fig. 7(a)] are performed, utilizing the COMSOL Multiphysics software [Fig. 7(b)]. The simulation model couples the electrical circuit interface (cir), the semiconductor interface (semi), and the moving mesh interface (ale) together. Take the ideal p–n junction

Published under an exclusive license by AIP Publishing

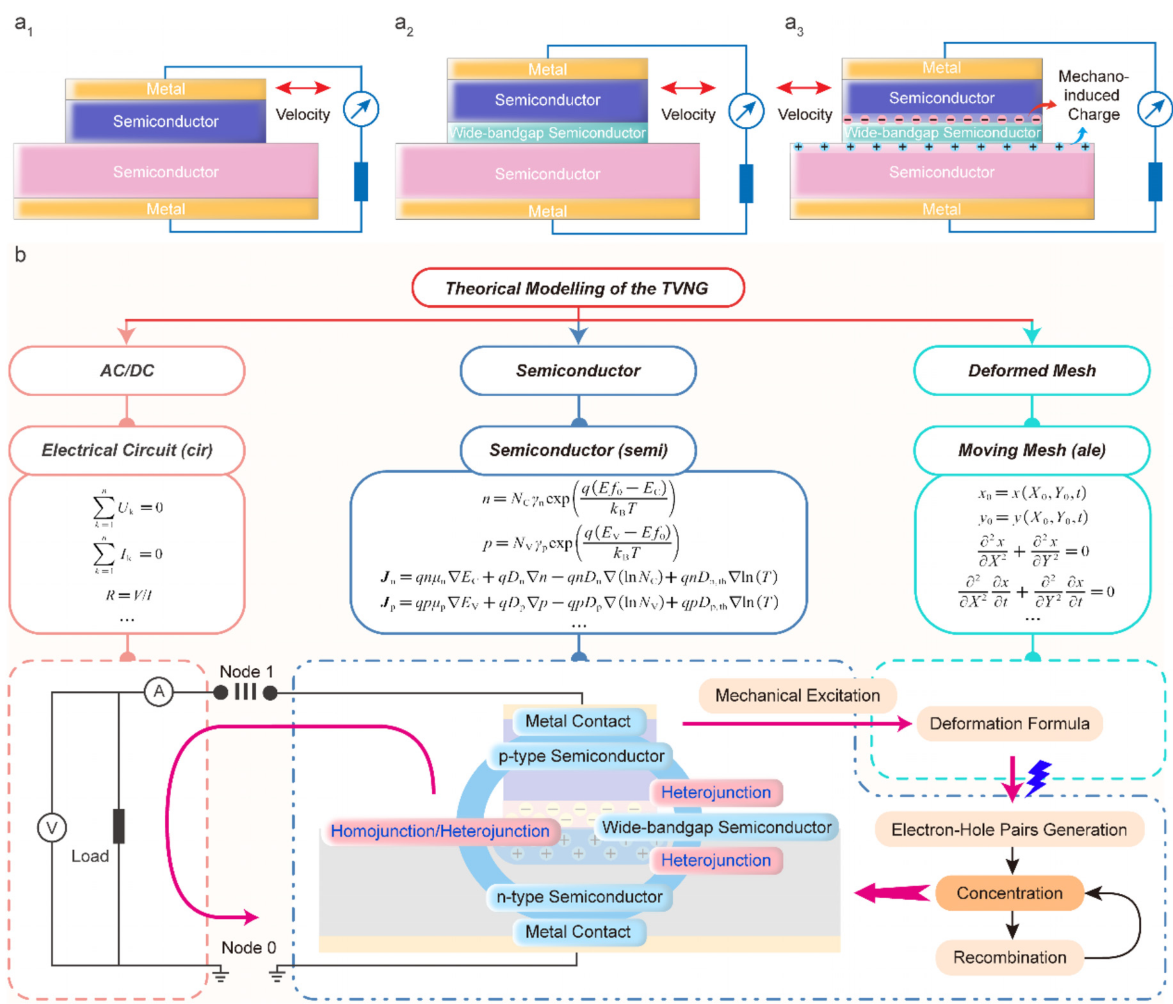

FIG. 7. The general simulation model of TVNG devices. Three typical configurations: (a_1) ideal p–n junction TVNG, (a_2) wide-bandgap semiconductor-sandwiched TVNG, and (a_3) mechano-induced electric field-dominated TVNG. (b) Theorical modeling of the TVNG using COMSOL Multiphysics Software couples three interfaces: the electrical circuit interface (cir) in the AC/DC module, the semiconductor interface (semi) in the semiconductor module, and the moving mesh interface (ale) in the deformed mesh module.

TVNG as an example. In the semiconductor interface, the stator is an n-type silicon doped with a donor concentration of N_D and the slider is a p-type silicon doped with an acceptor concentration of N_A. The dimensions of the slider and stator are denoted by L_1, H_1, L_2, and H_2, respectively. Electrodes are attached to the upper surface of the slider and the lower surface of the stator, and the two nonrectifying metal–semiconductor junctions are regarded as an ideal Ohmic contact. The lower electrode is grounded ($V = 0$ V), while the upper electrode is connected to the external circuit, with its potential equal to the voltage across the external circuit ($V = V_{cir}$). The circuit section is connected to a resistor, a Volt meter, and an Ampère Meter, respectively, which is to simulate loading, open-circuit, and short-circuit conditions. The movement equation of the slider is constructed in the moving mesh interface. All modeling parameters are available in the supplementary material (Tables I–III).

In semiconductor simulations, it is necessary to calculate the key physical quantities such as electric fields, carrier concentrations, electron and hole currents, and so on. The distribution of the electric potential is calculated from the Poison equation as follows:

$$\nabla \cdot (-\varepsilon_0 \varepsilon_r \nabla V) = \rho, \tag{16}$$

where the charge density ρ is contributed by the concentrations of all charged particles including electrons (n), holes (p), and ionized donors ($N_D{}^+$) and acceptors ($N_A{}^-$) as follows:

$$\rho = e\left(p - n + N_D^+ - N_A^-\right). \tag{17}$$

Note that the vacuum energy level is taken as a zero reference. From the Boltzmann statistical theory, n and p are determined by the Fermi level and conduction and valence bands

$$n = N_C \exp\left(-\frac{E_C - E_{Fn}}{k_B T}\right), \tag{18}$$

Published under an exclusive license by AIP Publishing
28 April 2024 01:10:04

$$p = N_V \exp\left(-\frac{E_{Fp} - E_V}{k_B T}\right), \tag{19}$$

where N_C and N_V represent the effective density of states in the conduction band and the effective density of states in the valence band. For silicon, $N_C = 1.04(T/300)^{3/2} \times 10^{19}\,cm^{-3}$. $N_C = 2.8(T/300)^{3/2} \times 10^{19}\,cm^{-3}$. The E_C and E_V are given by

$$E_C = -(eV + \chi), \tag{20}$$

$$E_V = -(eV + \chi + E_g). \tag{21}$$

In an indirect bandgap semiconductor such as silicon at low fields, trap-assisted recombination is usually the dominant contributor to the recombination of electrons and holes, which is characterized using the Shockley–Read–Hall model (supplementary material). The generation rates of electron–hole pairs are described in Eq. (11). Overall, the electron and hole concentrations related to generation and recombination can be obtained by solving the continuity equations as follows:

$$\frac{\partial n}{\partial t} = -\mu_n \nabla \cdot (n\boldsymbol{E}) + D_n \nabla^2 n + g_n - u_n, \tag{22}$$

$$\frac{\partial p}{\partial t} = -\mu_p \nabla \cdot (p\boldsymbol{E}) + D_p \nabla^2 p + g_p - u_p. \tag{23}$$

Then, the electron current density (J_n) and the hole current density (J_p) are determined by

$$\boldsymbol{J}_n = en\mu_n \boldsymbol{E} + eD_n \nabla n, \tag{24}$$

$$\boldsymbol{J}_p = en\mu_p \boldsymbol{E} + eD_p \nabla p. \tag{25}$$

SUPPLEMENTARY MATERIAL

See the supplementary material for the modeling details.

ACKNOWLEDGMENTS

This work was supported by the National Natural Science Foundation of China (Grant Nos. 62001031, 52192610, 51702018, and 51432005), the Youth Innovation Promotion Association, CAS, the Fundamental Research Funds for the Central Universities (Grant No. E0E48957), and the National Key R&D Project from Minister of Science and Technology (Grant No. 2016YFA0202704). The authors declare that they have no known competing financial interest or personal relationships that could have appeared to influence the work reported in this paper.

AUTHOR DECLARATIONS

Conflict of Interest

The authors have no conflicts to disclose.

Author Contributions

Xin Guo: Data curation (lead); Formal analysis (lead); Software (lead); Writing – original draft (lead). **Jing You:** Methodology (equal); Project administration (equal). **Di Wei:** Project administration (equal); Software (equal). **Jiajia Shao:** Supervision (equal); Writing – review & editing (equal). **Zhong Lin Wang:** Supervision (equal); Writing – review & editing (equal).

DATA AVAILABILITY

The data that support the findings of this study are available from the corresponding author upon reasonable request.

REFERENCES

[1] Z. L. Wang, "On Maxwell's displacement current for energy and sensors: The origin of nanogenerators," Mater. Today **20**(2), 74–82 (2017).
[2] Z. L. Wang, "From contact electrification to triboelectric nanogenerators," Rep. Prog. Phys. **84**(9), 096502 (2021).
[3] C. Zhang, W. Tang, C. Han, F. Fan, and Z. L. Wang, "Theoretical comparison, equivalent transformation, and conjunction operations of electromagnetic induction generator and triboelectric nanogenerator for harvesting mechanical energy," Adv. Mater. **26**, 3580–3591 (2014).
[4] B. Jia, M. Lei, Y. Zou, G. Qin, C. Zhang, L. Han, Q. Zhang, and P. Lu, "The electron transfer mechanism between metal and silicon oxide composites for triboelectric nanogenerators," Adv. Compos. Hybrid Mater. **5**, 3223–3231 (2022).
[5] D. Jiang, M. Lian, M. Xu, Q. Sun, B. B. Xu, H. K. Thabet, S. M. El-Bahy, M. M. Ibrahim, M. Huang, and Z. Guo, "Advances in triboelectric nanogenerator technology—applications in self-powered sensors, internet of things, biomedicine, and blue energy," Adv. Compos. Hybrid Mater. **6**, 57 (2023).
[6] J. Lin, J. Li, S. Feng, C. Gu, H. Li, H. Lu, F. Hu, D. Pan, B. B. Xu, and Z. Guo, "An active bacterial anti-adhesion strategy based on directional transportation of bacterial droplets driven by triboelectric nanogenerators," Nano Res. **16**, 1052–1063 (2022).
[7] C. Liu, L. Jiang, O. Yue, Y. Feng, B. Zeng, Y. Wu, Y. Wang, J. Wang, L. Zhao, X. Wang, C. Shao, Q. Wu, and X. Sun, "Thermal enhancement of gelatin hydrogels for a multimodal sensor and self-powered triboelectric nanogenerator at low temperatures," Adv. Compos. Hybrid Mater. **6**, 112 (2023).
[8] D. Sarkar, N. Das, M. M. Saikh, S. Roy, S. Paul, N. A. Hoque, R. Basu, and S. Das, "Elevating the performance of nanoporous bismuth selenide incorporated arch-shaped triboelectric nanogenerator by implementing piezo-tribo coupling effect: Harvesting biomechanical energy and low scale energy sensing applications," Adv. Compos. Hybrid Mater. **6**, 232 (2023).
[9] Q. Xu, Z. Wu, W. Zhao, M. He, N. Guo, L. Weng, Z. Lin, M. F. A. Taleb, M. M. Ibrahim, M. V. Singh, J. Ren, and Z. M. El-Bahy, "Strategies in the preparation of conductive polyvinyl alcohol hydrogels for applications in flexible strain sensors, flexible supercapacitors, and triboelectric nanogenerator sensors: An overview," Adv. Compos. Hybrid Mater. **6**, 203 (2023).
[10] Z. L. Wang and A. C. Wang, "On the origin of contact-electrification," Mater. Today **30**, 34–51 (2019).
[11] J. Liu, A. Goswami, K. Jiang, F. Khan, S. Kim, R. McGee, Z. Li, Z. Hu, J. Lee, and T. Thundat, "Direct-current triboelectricity generation by a sliding Schottky nanocontact on MoS2 multilayers," Nat. Nanotechnol. **13**(2), 112–116 (2018).
[12] R. Xu, Q. Zhang, J. Y. Wang, D. Liu, J. Wang, and Z. L. Wang, "Direct current triboelectric cell by sliding an n-type semiconductor on a p-type semiconductor," Nano Energy **66**, 104185 (2019).
[13] S. Jang, H. Shim, and C. Yu, "Fully rubbery Schottky diode and integrated devices," Sci. Adv. **8**, eade4284 (2022).
[14] X. Huang, X. Xiang, J. Nie, D. Peng, F. Yang, Z. Wu, H. Jiang, Z. Xu, and Q. Zheng, "Microscale Schottky superlubric generator with high direct-current density and ultralong life," Nat. Commun. **12**(1), 2268 (2012).
[15] J. Meng, C. Pan, L. Li, Z. H. Guo, F. Xu, L. Jia, Z. L. Wang, and X. Pu, "Durable flexible direct current generation through the tribovoltaic effect in contact-separation mode," Energy Environ. Sci. **15**(12), 5159–5167 (2022).
[16] J. Meng, Z. H. Guo, C. Pan, L. Wang, C. Chang, L. Li, X. Pu, and Z. L. Wang, "Flexible textile direct-current generator based on the tribovoltaic effect at dynamic metal-semiconducting polymer interfaces," ACS Energy Lett. **6**(7), 2442–2450 (2021).
[17] S. Lin, Y. Lu, S. Feng, Z. Hao, and Y. Yan, "A high current density direct-current generator based on a moving van der Waals Schottky diode," Adv. Mater. **31**(7), 1804398 (2019).
[18] S. Lin and Z. L. Wang, "The tribovoltaic effect," Mater. Today **62**, 111–128 (2022).
[19] L. Zhang, H. Cai, L. Xu, L. Ji, D. Wang, Y. Zheng, Y. Feng, X. Sui, Y. Guo, W. Guo, F. Zhou, W. Liu, and Z. L. Wang, "Macro-superlubric triboelectric nanogenerator based on tribovoltaic effect," Matter **5**, 1532–1546 (2022).

28 April 2024 01:10:04

Published under an exclusive license by AIP Publishing

[20]Z. Zhang, D. Jiang, J. Zhao, G. Liu, T. Bu, C. Zhang, and Z. L. Wang, "Tribovoltaic effect on metal–semiconductor interface for direct-current low-impedance triboelectric nanogenerators," Adv. Energy Mater. **10**, 1903713 (2020).
[21]M. Zheng, S. Lin, Z. Tang, Y. Feng, and Z. L. Wang, "Photovoltaic effect and tribovoltaic effect at liquid-semiconductor interface," Nano Energy **83**, 105810 (2021).
[22]M. Zheng, S. Lin, L. Xu, L. Zhu, and Z. L. Wang, "Scanning probing of the tribovoltaic effect at the sliding interface of two semiconductors," Adv. Mater. **32**(21), e2000928 (2020).
[23]S. Lin, X. Chen, and Z. L. Wang, "The tribovoltaic effect and electron transfer at a liquid-semiconductor interface," Nano Energy **76**, 105070 (2020).
[24]Z. Wang, Z. Zhang, Y. Chen, L. Gong, S. Dong, H. Zhou, Y. Lin, Y. Lv, G. Liu, and C. Zhang, "Achieving an ultrahigh direct-current voltage of 130 V by semiconductor heterojunction power generation based on the tribovoltaic effect," Energy Environ. Sci. **15**, 2366–2373 (2022).
[25]Z. Zhang, Z. Wang, Y. Chen, Y. Feng, S. Dong, H. Zhou, Z. L. Wang, and C. Zhang, "Semiconductor contact-electrification dominated tribovoltaic effect for ultrahigh power generation," Adv. Mater. **34**, 2200146 (2022).
[26]C. Ma, B. Kim, S.-W. Kim, and N.-G. Park, "Dynamic halide perovskite heterojunction generates direct current," Energy Environ. Sci. **14**, 374–381 (2021).
[27]Z. You, S. Wang, Z. Li, Y. Zou, T. Lu, F. Wang, B. Hu, X. Wang, L. Li, W. Fang, and Y. Liu, "High current output direct-current triboelectric nanogenerator based on organic semiconductor heterojunction," Nano Energy **91**, 106667 (2022).
[28]Y.-S. Lee, S. Jeon, D. Kim, D.-M. Lee, D. Kim, and S.-W. Kim, "High performance direct current-generating triboelectric nanogenerators based on tribovoltaic p-n junction with ChCl-passivated CsFAMA perovskite," Nano Energy **106**, 108066 (2023).
[29]J. Xia, X. Luo, J. Li, L. Zhu, and Z. L. Wang, "Wear-resisting and stable 4H-SiC/Cu-based tribovoltaic nanogenerators for self-powered sensing in a harsh environment," ACS Appl. Mater. Interfaces **14**(49), 55192–55200 (2022).
[30]Y. Lu, Z. Hao, S. Feng, R. Shen, Y. Yan, and S. Lin, "Direct-current generator based on dynamic PN junctions with the designed voltage output," iScience **22**, 58–69 (2019).
[31]Y. Lu, Q. Gao, X. Yu, H. Zheng, R. Shen, Z. Hao, Y. Yan, P. Zhang, Y. Wen, G. Yang, and S. Lin, "Interfacial built-in electric field-driven direct current generator based on dynamic silicon homojunction," Research **2020**, 5714754.
[32]J. Liu, M. Miao, K. Jiang, F. Khan, A. Goswami, R. McGee, Z. Li, L. Nguyen, Z. Hu, J. Lee, K. Cadien, and T. Thundat, "Sustained electron tunneling at unbiased metal-insulator-semiconductor triboelectric contacts," Nano Energy **48**, 320–326 (2018).
[33]M. Benner, R. Yang, L. Lin, M. Liu, H. Li, and J. Liu, "Mechanism of in-plane and out-of-plane tribovoltaic direct-current transport with a metal/oxide/metal dynamic heterojunction," ACS Appl. Mater. Interfaces **14**(2), 2968–2978 (2022).
[34]W. Qiao, Z. Zhao, L. Zhou, D. Liu, S. Li, P. Yang, X. Li, J. Liu, J. Wang, and Z. L. Wang, "Simultaneously enhancing direct-current density and lifetime of tribovotaic nanogenerator via interface lubrication," Adv. Funct. Mater. **32**(46), 2208544 (2022).
[35]C. Xu, J. Yu, Z. Huo, Y. Wang, Q. Sun, and Z. L. Wang, "Pursuing tribovoltaic effect for direct-current triboelectric nanogenerator," Energy Environ. Sci. **16**, 983–1006 (2023).
[36]R. Yang, R. Xu, W. Dou, M. Benner, Q. Zhang, and J. Liu, "Semiconductor-based dynamic heterojunctions as an emerging strategy for high direct-current mechanical energy harvesting," Nano Energy **83**, 105849 (2021).
[37]H. Zou, Y. Zhang, L. Guo, P. Wang, X. He, G. Dai, H. Zheng, C. Chen, A. C. Wang, C. Xu, and Z. L. Wang, "Quantifying the triboelectric series," Nat. Commun. **10**(1), 1427 (2019).
[38]X. Xu, Z. L. Wang, and Z. Yang, "Triboelectric junction: A model for dynamic metal–semiconductor contacts," Energy Environ. Sci. **17**, 149 (2024).
[39]G. Liu, J. Liu, and W. Dou, "Non-adiabatic quantum dynamics of tribovoltaic effects at sliding metal–semiconductor interfaces," Nano Energy **96**, 107034 (2022).
[40]M. B. Prince, "Silicon solar energy converters," J. Appl. Phys. **26**(5), 534–540 (1955).
[41]N. K. Elumalai and A. Uddin, "Open circuit voltage of organic solar cells: An in-depth review," Energy Environ. Sci. **9**(2), 391–410 (2016).
[42]D. A. Neamen, *Semiconductor Physics and Devices: Basic Principles* (McGraw-Hill, 2012).
[43]S. M. Sze and K. K. Ng, *Physics of Semiconductor Devices* (Wiley, 2021).
[44]B. Jayant Baliga, *Fundamentals of Power Semiconductor Devices* (Springer New York, 2008).
[45]Y. Chen, Z. Zhang, Z. Wang, T. Bu, S. Dong, W. Wei, Z. Chen, Y. Lin, Y. Lv, H. Zhou, W. Sun, and C. Zhang, "Friction-dominated carrier excitation and transport mechanism for GaN-based direct-current triboelectric nanogenerators," ACS Appl. Mater. Interfaces **14**, 24020–24027 (2022).

28 April 2024 01:10:04

Published under an exclusive license by AIP Publishing